Intermediate phases in binary and ternary alloys: a new perspective on semi-empirical bond constraint theory

2007 J. Phys.: Condens. Matter 19 455218

(http://iopscience.iop.org/0953-8984/19/45/455218)

IOP PUBLISHING JOURNAL OF PHYSICS: CONDENSED MATTER

J. Phys.: Condens. Matter **19** (2007) 455218 (20pp) doi:10.1088/0953-8984/19/45/455218

Intermediate phases in binary and ternary alloys: a new perspective on semi-empirical bond constraint theory

G Lucovsky[1] **and J C Phillips**[2]

[1] Department of Physics, North Carolina State University, Raleigh, NC 27695-8202, USA
[2] Department of Physics, Rutgers University, Piscataway, NJ 08854, USA

E-mail: lucovsky@ncsu.edu

Received 1 September 2007, in final form 2 September 2007
Published 24 October 2007
Online at stacks.iop.org/JPhysCM/19/455218

Abstract

This paper extends the scope of semi-empirical bond constraint theory, (SEBCT) and uses this extension to provide quantitative insights into the atomic scale bonding interactions for the two transitions that bracket intermediate phases (IPs) in binary and ternary alloys. Reversibility windows have usually been defined in terms of the average bonding coordination, r_c (also, N_{av}, $\langle r \rangle$), and show considerable *scatter* between different alloys when displayed in this way. This paper analyzes and plots these transitions in terms of the average number of bonding constraints/atom, n_c (also C_{av}), and thereby provides important insights into the extent to which SEBCT must be modified by either *extending*, or *contracting* the force field with respect to the 2-body bond-stretching and 3-bond-bending valence forces of the original SEBCT formulation. These modifications include (i) broken bond-bending constraints that reduce n_c below the level determined from stretching and bending constraints of the SEBCT, and (ii) additional forces due to repulsions between non-bonding lone-pair orbitals on two-fold coordinated Se, three-fold coordinated As, and terminal or one-fold coordinated I atoms that add additional constraints to the SEBCT counting. These modifications identify the bonding interactions that give rise to the scatter in the r_c-based plots, and then use the IP plots based on r_c to provide a way of determining whether broken or additional constraints move the window threshold, respectively above or below the SEBCT value of 2.4.

1. Introduction

A semi-empirical bond constraint theory, SEBCT, based on valence force field 2-body bond-stretching and 3-body bond-bending forces, has identified several important and relatively simple relationships between (i) mean-field local atom-specific bonding coordinations, and

bonding constraints, and (ii) the ease of glass formation in chalcogenide alloy systems [1]. This approach has demonstrated that descriptions of non-crystalline solids using the *mean-field* atomic coordination, or equivalently the average number of bonds/atom, r_c (also N_{av} or $\langle r \rangle$), and the *mean-field* or average number of valence bonding stretching and bending constraints/atom, n_c (also C_{av}), provide a novel, and also an elegant way to separate bulk chalcogenide and glasses and into (i) very good, or (ii) marginal/poor glass formers in the context of bulk-quenching methods. This approach has also been extended to oxide glasses, as well as silicate classes that contain ionic oxides as well in glass forming silicate compositions, e.g., Na_2O and CaO alloys with SiO_2 as in window glass [2]. This same approach has also been extended to thin film chalcogenide and oxide compound and alloy compositions [3–5]. However for thin films it is important to verify that the films are single phase, and have been annealed at a sufficiently high temperature, e.g., approximately 2/3 of the glass transition temperature, T_g, to relax their bonding arrangements so that they are essentially the same as bulk-quenched glasses.

For three-dimensional chalcogenide and oxide network glasses and thin films, a value of n_c equal to the number of degrees of freedom for atomic motions, or equivalently the network dimensionality of three (3) has provided a criterion for identifying compounds such as $As_2S(Se)_3$, and alloys such as $GeSe_4$ as good glass formers in general agreement with experiment [1]. Based on the 2- and 3-body force field representation, the value of $n_c = 3$ corresponds to a mean-field coordination of $r_c = 2.4$. Using these metrics, chalcogenide glasses and thin films have been organized into three different categories: (i) *flexible*, also more commonly designated as *floppy* or under coordinated, with $r_c < 2.4$ and $n_c < 3$, (ii) *ideal*, or optimally coordinated with $r_c = 2.4$ and $n_c = 3$, and finally (iii) *stressed rigid* or over coordinated with $r_c > 2.4$ and $n_c > 3$. Glasses and thin films with $n_c < 3$, or $n_c > 3$ generally contain significant concentrations of intrinsic bonding defects, e.g., broken or dangling bonds, which in many instances are too high for electronic device applications as in plasma deposited Si_3N_4 thin films [3, 4]. However, it is well known that incorporating relatively high concentrations of bonded H into to Si_3N_4 of the order to 20–30 at.% will compensate and neutralize dangling bond defects on both Si and N atoms, and thereby reduce the defect densities of electronically active traps [4].

Based on Maxwellian theory and Lagrangian constraints [6] a single and abrupt transition between floppy and stressed-rigid glass alloy compositions is expected, e.g., at $x = 0.2$ in Ge_xSe_{1-x}. This is the composition at which $r_c = 2.4$ and $n_c = 3$. However the abrupt aspect of these transitions was not supported by theory [7], and this expectation has been verified by the extensive experiments of Boolchand and co-workers as well [8].

This paper identifies two important force-field extensions that go beyond the original SEBCT formulation in terms of bond-stretching and bond-bending forces. These provide a basis for understanding systematic differences in the widths of IPs, and the values of r_c that bracket these IP windows, and additionally provide a way of *encoding* the r_c plots to determine if broken constraints, or additional constraints apply to a particular alloy system. Boolchand and co-workers have used the values of $r_c(1)$ for the onset of the IP, $r_c(2)$ for the end of the IP, and $\Delta r_c(W) = r_c(2) - r_c(1)$ to define the IP window width [9]. This paper also defines and compares IP windows using the *corresponding* constraint counting metrics, $n_c(1)$, $n_c(2)$ and $\Delta n_c(w)$. This provides a complementary approach that leads to a better understanding of the relationship between chemical bonding in floppy and stressed-rigid networks that bracket the IP window, and the chemical bonding self-organizations (CBSOs) that are important in determining the widths of the IP windows.

This new approach is based on two important extensions to SEBCT that are related to the nature of the constraining forces that contribute to n_c and are discussed in section 2.

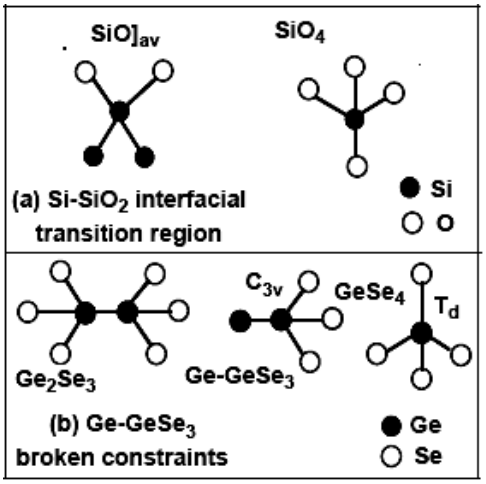

Figure 1. Schematic representations of tetrahedral bonding arrangements. Top: local bonding in SiO as discussed in [10]. This portion of the figure displays the average O_2–Si–Si_2 bonding as well as a reference Si–O_4 bonding. Bottom: the local Se_3–Ge–Ge–Se_3 bonding of the chemically order Ge_2Se_3 alloy, as well as the bonding of a completely symmetric Ge–Se_4 arrangement, T_d symmetry, and a reduced symmetry Ge–Ge–Se_3 arrangement, C_{3v} symmetry.

These force-field modifications include (i) broken bond-bending constraints, which generally result from strain reducing chemical bonding self-organizations that minimize bond strain at the expense of reductions in configurational entropy, and/or (ii) longer range forces that are associated with repulsive interactions between electrons in lone pair orbitals on two and three-fold coordinated alloy atoms, e.g., Se and As, respectively, as well as one-fold coordinated terminal halogen atoms such as I.

2. Modifications to bonding constraint counting

2.1. Broken bond-bending constraints

The concept of *broken* bond-bending constraints for tetrahedrally coordinated Si with two O and two Si bonding neighbors was first addressed by Lucovsky and Phillips in [10]. That paper discussed on the Si–O bonding in the interfacial transition region between Si and SiO_2 in Si metal–oxide–semiconductor (MOS) field effect transistor devices. Figure 1(a) displays the *average* local bonding arrangement, O_2–Si–Si_2, in the interfacial transition region between Si and SiO_2, as well as a reference Si–O_4 bonding arrangement for SiO_2. In [10] it was noted that 'the number of bond-bending constraints associated with this average bonding can then be determined from symmetry considerations.' In SiO, 'there is' on average 'one Si–Si–Si bond angle, and one O–Si–O bond angle; each of these symmetrical angles can be constrained at the sp^3 tetrahedral angle of approximately 110°. On the other hand, it is unlikely that the asymmetric O–Si–Si bond angles will be constrained' to the same degree 'because the local *energy gaps* are associated with O–Si and Si–Si bonds. These gaps are sufficiently different so that the Pauling bonding resonance responsible for bond-bending forces is expected to be negligibly weak compared to the resonances responsible for the bond-bending forces associated with the symmetric Si–Si–Si and O–Si–O bond angles.' Proceeding in this way they went on to conclude that 'based on this analysis, the number of constraints per SiO formula unit can now

be calculated. There are three stretching constraints, one Si–Si–Si-bonding constraint, and one O–Si–O-bending constraint that must be counted. 'Finally, there is one additional constraint associated with the angle between the normals to the Si–Si–Si and O–Si–O bonding planes. This gives six constraints per SiO, or equivalently 3 constraints per atom, matching the atomic degrees of freedom. This leads to the unexpected conclusion that the ultra-thin, interfacial SiO_x layer is effectively strain free, and therefore provides an ideal continuous transition between the tensile and compressive stress respectively of the Si substrate and SiO_2 dielectric.' The same type of analysis also applies to the isoelectronic GeSe average bonding structure, and this approach has additionally been applied to Ge–Se_4 and Ge–Ge–Se_3 molecular arrangements that are the mean-field arrangements for $GeSe_2$ ($x = 0.33$) and Ge_2Se_3 ($x = 0.40$), respectively [6].

We first apply this counting to a local bonding arrangement that is occurs the Ge–Se alloy system for the composition Ge_2Se_3, or equivalently $Ge_{0.4}Se_{0.6}$ [11]. Figure 1(b) gives a schematic representation of the Se_3–Ge–Ge–Se_3 bonding of the chemically order Ge_2Se_3 alloy, as well as the bonding of a completely symmetric Ge–Se_4 arrangement, and a reduced symmetry Ge–Ge–Se_3 arrangement. Applying the same criterion to symmetric Se–Ge–Se, and asymmetric Ge–Ge–Se-bending motions, the bond constraints for symmetric geometries are retained, while for asymmetric geometries they are broken and not counted. The bonding changes in figure 1(b) lead to a reduction in local site symmetry of the Ge atom from T_d in a completely symmetric Ge–Se_4 arrangement to C_{3v} symmetry in a Se–Ge–Se_3 with reduced symmetry; this reduces the number of bond-bending constraints [6, 12]. By considering the normal mode motions of the respective structures, the number of bond-bending constraints is reduced from 5 for the symmetric Ge–Se_4 arrangement to $\sim$2.5 for the symmetric Se_3–Ge–Ge–Se_3 arrangement. Two of the broken constraints are associated with Ge–Ge–Se-bending modes, and the 0.5 constraint involves the asymmetry in the additional constraint associated with the angle between the normals to the Ge–Ge–Se and Se–Ge–Se bonding planes. This is equivalent to recognizing that the only five the six bond-angles centered on the Ge atom at the center of the Ge–Ge–Se_3 cluster are independent; the factor of 0.5 takes this into account in the spirit of mean-field constraint counting. The same result can be obtained by an analysis of the changes in normal mode motions in going from XY_4 to X_2Y_3 tetrahedral molecules [13], and eliminating bending motions that involve asymmetric triads of atoms centered on the X atom at the center of the reduced symmetry tetrahedral bonding arrangement.

2.2. Repulsive bonding constraints

This sub-section develops a model for understanding the effects of the relatively strong repulsive forces between the electrons in (i) lone-pair orbitals on nearest-neighbor network As and Se atoms in As–Se and Ge–As–Se alloys, and (ii) lone pair Se orbitals and terminal I atoms in Ge–Se–I alloys. Figure 2(a) includes schematic representations of the bonding arrangements in As_xSe_{1-x} alloys. The mean-field bonding at the compound composition, As_2Se_3, is shown in a plan view representation with three different geometric arrangements for the lone pair electrons on the As atoms, in (i) *up–up*, (ii) *up–down* and (iii) *down–down* geometries. Figure 2(b) indicates the mean-field bonding in the As_2Se_5 ($r_c = 2.29, x_c = 0.286$) composition; this will be addressed in greater detail later on in this sub-section.

The importance of the repulsive forces involving non-bonding pairs on two and three coordinated network atoms, and on halogen terminators has been understood in molecular bonding chemistry for more than 30 years, and is integrated into the valence shell electron pair repulsion (VSEPR) model [14, 15]. The VSEPR model has been used to predict the *shapes of small molecules*, generally with from three to seven atoms and identifies the significant contributions of non-bonding lone-pair electrons in contributing to asymmetric molecular

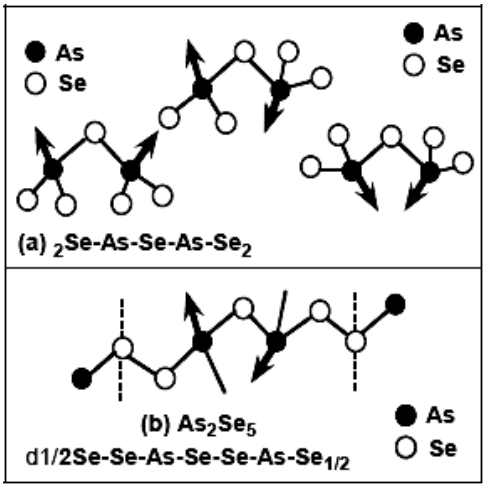

Figure 2. Plan view schematic representations of bonding arrangements in As_xSe_{1-x} alloys: (a) The mean-field bonding at the compound composition, As_2Se_3 indicating three different geometric arrangements of the lone pair electrons on the As and Se atoms: (i) up–up, (ii) up–down and (iii) down–down. (b) The mean-field bonding in the As_2Se_5 ($r_c = 2.29$, $x_c = 0.286$) composition. The solid arrows represent the orientations of the As lone pairs. The lone pairs on the Se atoms are normal to the plane of the diagram.

structures such as XeF_6. This model, based on total energy calculations, in particular on an observation that bonding arrangements between the 2-electron sigma (σ) and pi (π) bonds, and non-bonding lone pairs of near-neighbor atoms in a molecule will adopt a geometry in which the distance between the electron pairs in σ- and π-bonds and the lone-pair electrons is optimized by reducing repulsive interactions. These repulsions are significantly larger than repulsions between electrons in bonding orbitals due to the geometric differences between the stronger confinement of electrons between (i) σ- and π-bonds and (ii) lone-pair orbitals. The repulsions result in a molecular geometry with the lowest total energy that is a balance between electronic energy, and bond-strain energy, and thereby generate a *significant constraint* with respect to molecular structure. The theory allows one to predict which hybridization, or geometry of the central atom best describes this optimization balance.

Applied to network non-crystalline solids, this allows us to identify bonding constraints that go beyond the elementary 2-body bond stretching and 3-body bond-bending forces of the original formulation of the SEBCT. This is based on an analogy between distortions in molecules that include non-bonding pairs, and additional constraints in non-crystalline network solids that include non-bonding lone pairs on two different atomic constituents, e.g., As and Se in in As_xSe_{1-x} and $Ge_xAs_ySe_{1-x-y}$ alloys, and lone pairs on one atomic constituent and a terminal halogen atom, e.g. Se and I, respectively, in $Ge_xSe_yI_z$. In the discussions of bonding constraints that follow, one additional constraint/atom will be added to each atom involved in a lone pair repulsive interaction between two different atoms, or in an interaction between a lone-pair atom, Se, and a halogen atom, I. This paper does not address (i) alloys that include As–As bonds, nor does it include (ii) include constraints between lone pairs in Se–Se bonds that are assumed to have always a non-parallel alignment of non-bonding lone-pair atoms. This alignment is characteristic of the local bonding arrangements of Se atoms in amorphous Se, monoclinic Se and trigonal Se [16], as well as other molecules, and carries over to Se rich glasses, e.g. Ge_xSe_{1-x} alloys with x between approximately 0.05 and 0.20, i.e. in a regime where the alloy is clearly not diphasic with an Se_8 molecular constituent [19].

3. The first intermediate phase for Ge_xSe_{1-x} alloys

Boolchand and co-workers [17] have demonstrated that an IP window in Ge_xSe_{1-x} alloys, extends from (i) the onset of local rigidity in the context of a mean-field description at $x_c(1) \sim 0.20$ with $r_c(1) \sim 2.4$, to a composition that (ii) defines the beginning of a stressed-rigid alloy regime at $x_c(2) \sim 0.26$ with $r_c(2) \sim 2.52$. The IP window width was initially estimated from Raman scattering measurements; however, a better and more accurate estimate of the positions of the two transitions that bracket the IP has been obtained form experiments that have addressed reversible heat flow [18]. The value of $n_c(1)$ at the first transition marks the onset of rigidity, and the alloy is not as yet stress; $n_c(1)$ has the expected value of 3.0 at this first transition. This value is consistent with the bonding constraints on the Ge and Se being due primarily to 2-body bond-stretching and 3-body bond-bending forces, with $n_c(\text{Se}) = 2$, and $n_c(\text{Ge}) = 7$. The value of $n_c(2)$ at the second transition to a stressed-rigid phase as determined from the same valence force field approximation is 3.3. However, at this composition, Raman spectra indicate a small fraction of edge sharing (ES), as well as corner sharing (CS) tetrahedra, and additional constraints associated the ES arrangements are possible [19]. In the ES configuration there are 4-atom rings, Ge–Se–Ge–Se, and the lone pairs on the Se atoms are in a parallel alignment. The concentration of the ES units can be neglected for the first transition from floppy to rigid, so that constraint counting need only consider stretching and bending forces [19].

Based on the Raman spectra in [19], the increased rigidity of the small Ge–Se–Ge–Se ring structure can be taken into account by increasing the number of constraints by one (1) for the Se atom pair within the ring, or equivalently by the addition by 0.5 constraints per Se atom. This is the only instance where we specifically identify a constraint associated with Se–Se lone pairs that are in Se–Ge–Se arrangements. As noted above, the small ring bonding topology forces the long pairs into a nearly parallel alignment that is known to generate a pair of band edge defects in amorphous Se [20]. For the Ge concentration of $x_c(2) = 0.26$ at the second transition, ∼20% of the Se atoms are in ES arrangements, so that the mean-field value of $n_c(\text{Se})$ is increased from 2 to ∼2.1. Taking this additional partial constraint into account increases the value of $n_c(2)$ for the second transition from 3.3 to 3.37, increasing the IP window width from $\Delta n_c(W) = 0.3$ to $\Delta n_c(W) = 0.37$. There are no changes in $r_c(2)$, or $\Delta r_c(W)$.

Several papers have addressed the width of this IP regime from modeling perspective, but not have addressed it in the context of the changes in bonding that must occur within the IP to account for the remarkable properties within that regime: (i) the absence of aging, i.e. no changes in time with properties such as T_g, and (ii) the reversibility of heat flow [21]. Since a mean-field description is not applicable in this IP regime [22], a different approach is required for addressing the microscopic and macroscopic aspects of bonding within the IP regime.

The relatively simple bonding model presented below provides important insights into the underlying microscopic bonding chemistry changes in this first IP regime in the Ge_xSe_{1-x} alloy system in *by looking into* the IP window from the respective floppy and stressed-rigid phases that bracket the IP. Unlike the bonding within the IP window that is determined by CBSOs that are outside of the domain of a mean-field approach, the bonding in these bracketing phases can be addressed in terms of a mean-field description. This approach will be addressed and implemented following the schematic representations of the IP windows addressed below.

Figures 3(a) and (b) contain schematic representations of the IP windows in Ge_xSe_{1-x} alloys plotted respectively as functions of $r_c(i)$ and $n_c(i)$ that include: (i) the values of $r_c(1)$ and $r_c(2)$, respectively at the edges of floppy and stress-rigid regimes that bracket the IP, and similarly for (ii) the values of $n_c(1)$ and $n_c(2)$ that bracket the IP regime. The plot in figure 3(a) includes values of r_c within the IP as well. However, within the IP, the relationship between n_c

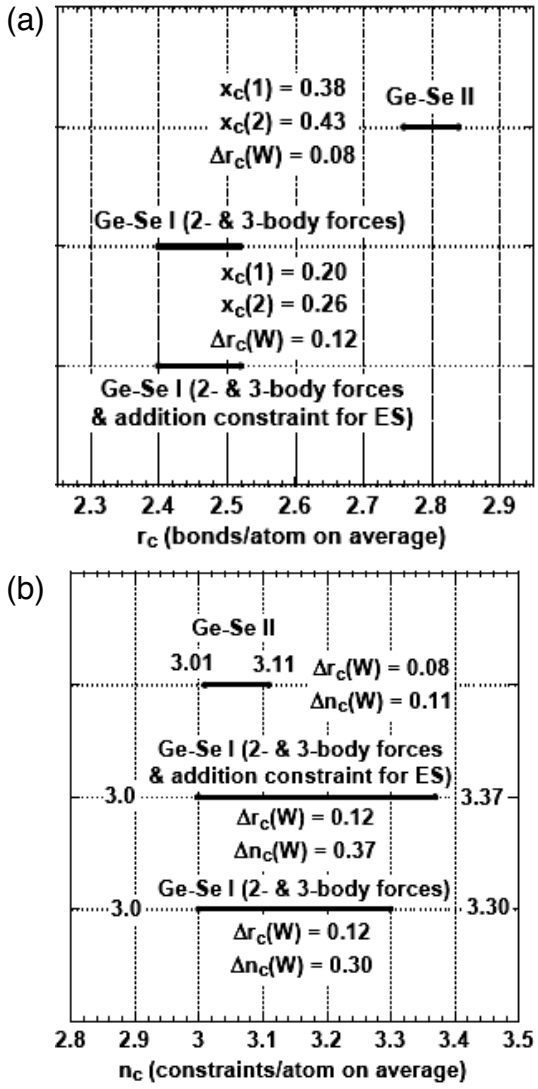

Figure 3. Schematic representation of IP regimes in the Ge_xSe_{1-x} alloy system. (a) Displayed as function of r, and (b) as a function of n. These plots include the first IP in Ge–Se alloys that begins at $x \sim 0.2$ ($GeSe_4$) under two different assumptions (a) 2- and 3-body stretching and bending forces, and (b) with an additional repulsive constraint on the Se atoms, associated with edge-shared tetrahedra, at the second transition. The r_c plot also includes the second IP (labeled II) that is centered at the composition Ge_2Se_3 ($x \sim 0.40$) and the model calculations include ES. The IP region for this alloy is included in the n_c plot; however it must be understood that $n_c > 3$ in both of the alloy regimes that bracket this IP.

and r_c developed in [1], and shown in equation (1),

$$n_c = 2.5r_c - 3 \tag{1}$$

does not apply, since n_c within the IP has an effective and constant value of 3. The plot in figure 3(a) indicates the IP window extends from $r_c(1) = 2.4$ ($x_c(1) = 0.20$) to $r_c(2) = 2.52$ ($x_c(2) = 0.26$) for IP window widths: $\Delta r_c(W) = 0.12$, and $\Delta x_c(W)$ of 0.06. The plot

in figure 3(b) indicates an IP window extends from $n_c(1) = 3.0$ to $n_c(2) = 3.37$ for a window width, $\Delta n_c(W) = 0.37$. However, as noted above, the x-axis values in the n_c plot are not to be construed as applying within the IP window.

The closely related Ge_xS_{1-x} alloy system has not been addressed, primarily because of the inherent diphasic nature of that system for values of $x < \sim 0.25$ or $1 - x > 0.75$. For these low Ge, high S content alloys, the glasses, and *properly* annealed thin films are inherently diphasic with a secondary molecular constituent phase, S_8, and a primary network phase [23].

4. The second glass forming regime for Ge_xSe_{1-x} alloys: is it an IP window?

The section addresses a second possible glass-forming regime in the Ge_xSe_{1-x} alloy system centered at $x \sim 0.4$ [1, 6, 12]. This is separated with respect to excellent glass formation at lower Ge concentrations ($x \sim 0.2$–0.26) by a poorer glass forming regime centered at the compound composition $GeSe_2$ or $x = 0.33$ [1]. This second glass-forming regime is *embedded* between two stressed-rigid regimes with $n_c \sim 3.7$ for $GeSe_2$, and more than 3 for a 43% Ge content with a *nominal composition* of Ge_3S_4; however, there is no known compound with this particular '3–4' stoichiometry.

The existence of marginally good glass formation at the composition Ge_2Se_3 or $x = 0.4$, demonstrates that the homopolar Ge–Ge bond does not introduce an additional or significant bonding constraint, but does, in point of fact, reduce the value of n_c at this composition [6, 11, 12]. This is addressed using the concept of symmetry determined broken constraints first introduced in [10], and discussed earlier in section 2.1. The formation of homopolar Ge–Ge bonds reduces the symmetry of the local Ge bonding symmetry from *ideal tetrahedral* with four *equivalent* Se nearest neighbors to *distorted tetrahedral* with three Se and one Ge nearest neighbor, i.e. from T_d to C_{3v} symmetry (see figure 1(b)). The Se atom bonding remains 2-fold coordinated to Ge nearest-neighbor atoms. The reduction in symmetry of the Ge atoms, changes the symmetry of the bond-bending vibrations [12, 13] and thereby removes some of these bending modes from the constraint counting arena, accounting for the second glass forming regime. There are two bond-stretching, and five bond-bending constraints for 4-fold coordinated Ge with full tetrahedral T_d symmetry [1, 2]; three are triply degenerate F-modes and two doubly degenerate E-modes [13]. As noted in section 2.1, there is significantly larger bond-bending force constant for the bending mode of a symmetric Se–Ge–Se group, than for an asymmetric Ge–Ge–Se group. Proceeding in this way, the number of effective or un-broken bond-bending constraints for the C_{3v} Ge tetrahedral molecular environment in Ge_2Se_3 is reduced from 5 to $\sim$2.5 [6, 12, 13]. The bond-stretching force constraints involve only nearest-neighbor pairs; there are 2 constraints per Ge atom in a 4-fold coordinated bonding environment independent of the nature of the neighbors and the symmetry. The total number of constraints per Ge atom is thereby reduced from 7, or 5 bending + 2 stretching for a T_d symmetry, to $\sim$4.5, i.e. $\sim$2.5 bending +2 stretching for a *distorted* tetrahedral arrangement as in the Ge_2Se_3 molecular fragment (see figure 1(b)). This reduction can also be addressed from the perspective of the local molecular structure in which there are six bond angles incorporated with a Ge-centered tetrahedron with either T_d or C_{3v} symmetry. Five of the these angles are independent, and the 6th angle is then determined by geometrical considerations, thereby accounting for 5 constraints. In the language of mean-field theory, this can be stated differently by using the Pauling concepts of resonance for the constraints. In this representation there are five constraints, but these resonate between all of the bonds, so any one of these can be active as a constraint. Reducing the symmetry does change this, but changes the nature of the resonance; based on this the combination of 3 symmetric Se–Ge–Se, and 3 asymmetric Ge–Ge–Se bondings is equivalent to a mean-field reduction to 2.5 bending constraints.

Returning to constraint counting, the number of bonds per atom at the Ge_2Se_3 composition is $r_c = 2.8$, and the number of constraints from equation (1) = 4.5. However, since the number of bonding constraints per atom is reduced because of the broken bond-bending constraints, and the reduction of bond-bending constraints from 5 to ∼2.5, the value of n_c is reduced according, and is equal to 3, matching the degrees of freedom in the space-filling three-dimensional network [1].

The experimental range of secondary glass formation in this system is from $x \sim 0.38$ to ∼0.4, and it is necessary to determine experimentally whether this is indeed an IP window; for example by determining whether the heat flow at T_g is reversible. However, if it were indeed an IP, it would be qualitatively different than the IP that begins 20% Ge and terminates at ∼26% Ge. That IP is bounded for the low composition transition by a floppy region, and for the high composition range by a stressed rigid regime (see figures 3(a) and (b)). If an IP window were to exist at between ∼38 and 42% Ge, it would be bounded instead by stressed-rigid regimes at both the low and high Ge content boundaries.

The values of n_c have been estimated for concentrations of $x = 0.38$ and 0.42 by assuming pseudo-binary alloy mixtures of $GeSe_2$ and Ge_2Se_3 for $x = 0.38$, and Ge_2Se_3 and GeSe for $x = 0.42$. This analysis gives values of n_c that bracket the value of 3 for $x = 0.4$ by higher values of n_c: $n_c(0.38) = 3.2$ and $n_c(0.42) = 3.13$. This alloy regime is represented in the r_c plot in figure 3(a), but it must be remembered that in the n_c plot in figure 3(b), the values of n_c within an IP window do not apply.

5. The intermediate phase for As_xSe_{1-x} alloys

The next issue to be addressed is: are the concepts and model presented above *unique* to Ge_xSe_{1-x}, and other 4–2 systems such as Si_xSe_{1-x}, in which the valence force field bond-stretching and bond-bending constraints, or does it apply more generally to other systems in which the reported IP windows are quantitatively different, and therefore require significant force field modifications [9]? This question is addressed and answered below as it applies to the primary, and only IP window in the As_xSe_{1-x} alloy system [9].

Figures 4(a) and (b) present schematic representations of the IP regimes in the Ge_xSe_{1-x} and As_xSe_{1-x} alloy systems as functions of r_c in (a) and n_c in (b). This plot includes the first Ge_xSe_{1-x} IP window ($r_c(1) = 2.4$) with the ES force at the second transition, and the second Ge_xSe_{1-x} IP centered at $r_c = 2.8$. For the 3–2 As_xSe_{1-x} alloys, the onset of the IP phase, as determined by the Boolchand group [9], occurs at a reduced of $r_c(1) \sim 2.3$, lower than 2.4, and also within the floppy regime with respect to the Lagrangian constraints of the SE-BCT. The value of $r_c(2)$ is ∼2.37, which is also less than 2.4, the ideal bond density for the SEBCT force field. The issue is: why is this entire IP window shifted to lower values of r_c? The qualitative answer is straightforward: there must be additional constraints operative in these 3–2 (As–Se) alloys that are not present in the 4–2 (Ge–Se) alloys, either in the first or second IPs labeled I and II in figures 3 and 4. These additional constraints will shift the value of r_c that corresponds to $n_c = 3$ to a lower As concentration $x_c(1)$, and therefore a lower value of $r_c(1)$ as well.

The microscopic, or chemical bonding specific answer is in the differences in the electronic structure between 3-fold coordinated As and 4-fold coordinated Ge [22]. Both As and Ge bonding obey the 8-N role in the respective As_xSe_{1-x} and Ge_xSe_{1-x} alloy systems [24]. In the spirit of the VSEPR model, this rule implicitly includes ideal or distorted tetrahedral arrangements of σ-bonds and lone-pair orbitals: e.g. Ge makes 4σ-bonds, and As 3 makes σ-bonds and has a lone-lone pair in the fourth position of a distorted tetrahedral geometry [14, 15]. The VSEPR repulsions reduce the angles between the σ-bonds to less than the tetrahedral value of ∼110° in the $As–Se_{3/2}$ pyramidal bonding arrangements with C_{3v} symmetry. Se is

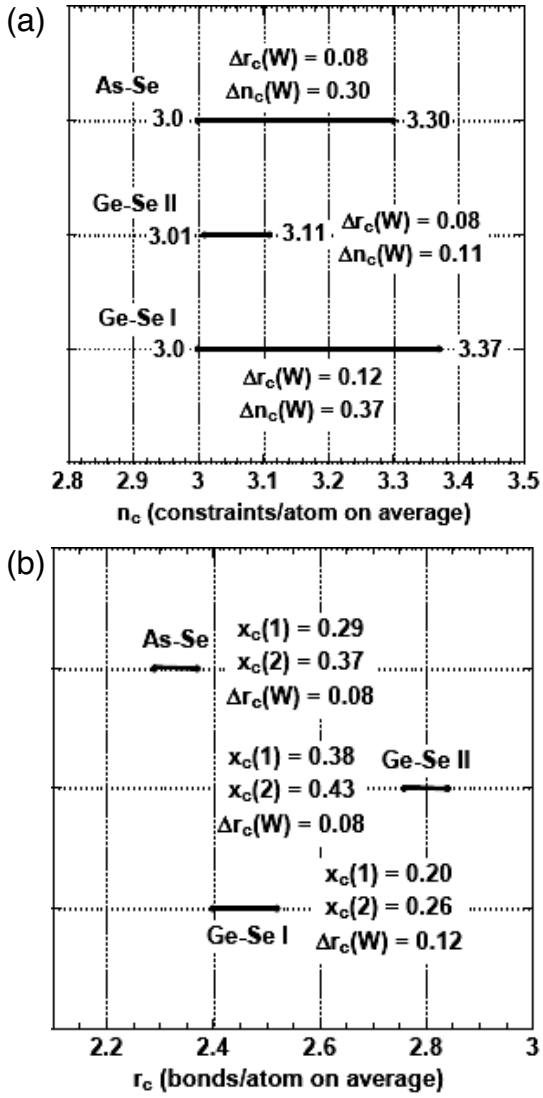

Figure 4. Schematic representation of IP regimes in the Ge_xSe_{1-x} and As_xSe_{1-x} alloy systems as functions of r in (a) and n in (b). This plot includes the first Ge_xSe_{1-x} IP window ($r_c(1) = 2.4$) with the ES force at the second transition, and the second Ge_xSe_{1-x} IP ($r_c(1) = 2.8$) is included as well.

qualitatively different; there are two σ-bonds and one lone-pair orbital that are derived almost entirely from atomic p-states angles between 90° and 100°; the second lone pair is derived from s-states, and adds a symmetric contribution to the electron density.

The results of electronic structure calculations for As_2S_3 and As_2O_3 are included in figures 5(a) and (b) [25, 26], and indicate that repulsions between lone pair orbitals on As and S atoms in As_2S_3, and As and O atoms in As_2O_3, have a significant on the local molecular structure. Figure 5(a) contains a plot of the normalized energy for As_2S_3 as a function the As–S–As bond angle, and the 'up–up', 'down–down' and 'down–up' notation are based on

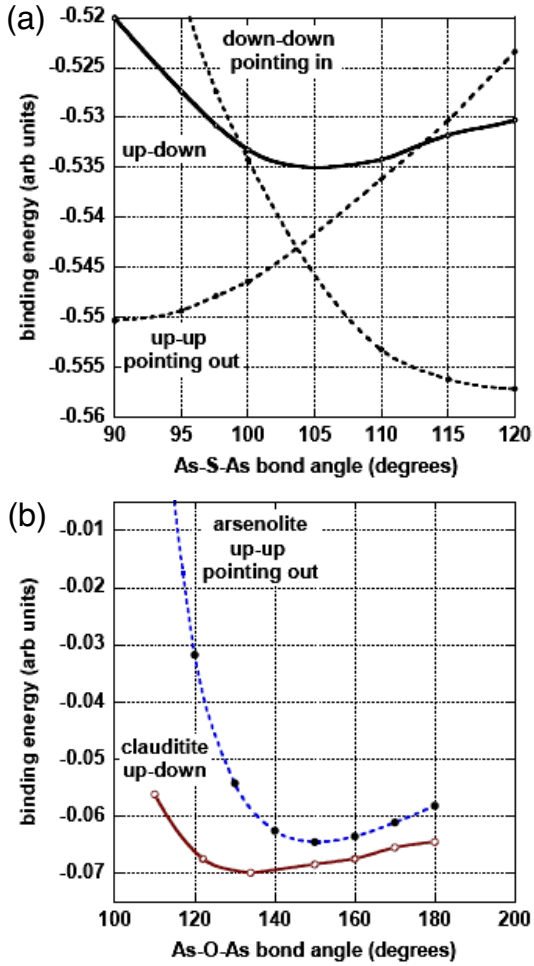

Figure 5. (a) Normalized energy for As_2S_3 as a function the As–S–As bond angle. (b) Normalized energy for As_2O_3 as a function the As–O–As bond angle.

(This figure is in colour only in the electronic version)

the schematic plan view diagrams in figure 2. The plot in figure 5(a) demonstrates the strong dependence of energy on the relative orientation of the As–$S_{2/2}$ groups that bridge the S atoms in the As–S–As bonds. It is obvious from this plot that there are strong constraining forces in this 3–2 chalcogenides that are associated with repulsive interactions between the As lone-pair electrons that bridge the central S atom. The bond angle for the 'up–down' arrangement of As lone pair orbitals is in excellent agreement with experiment, while the energy dependence of the 'up–up' and 'down–down' arrangements give markedly unphysical answers. Figure 5(b) illustrates a similar plot for As_2O_3 that includes (i) the 'up–down' bonding within the two-dimensionally extended multi-atom layers of the clauditite crystal with a *mica-like* structure, and (ii) the 'up–up' bonding the approximately spherical As_3O_6 molecule that is the basis for the molecular crystal arsenolite [27]. This calculation supports the empirical observation that the preferred structure of As_2O_3 is the clauditite crystal, rather than the molecular arsenolite crystal based on the As_3O_6 molecule.

The strong repulsive forces that are have been invoked to explain the energy plots in figures 5(a) and (b) cannot be addressed in the spirit of valence force field bending and stretching constraints alone. It will be demonstrated that including an *equivalent bonding constraint* for As lone-pair repulsions explains the experimental results for the As_xSe_{1-x} IP window that are based on applying the Ge_xSe_{1-x} bonding model of bridging single and dimer pairs of Se atoms as a basis for As_xSe_{1-x} alloys as well.

At the $GeSe_4$ or $x = 0.20$ Ge composition, on average, each pair of Ge atoms is separated in all four tetrahedral directions by two Se atoms. Using this bonding metric as a *template for the network connectivity* in As_xSe_{1-x} alloys requires that there be at least two As–Se–Se–As linkages for each As atom pair that bridges a one Se atom As–Se–As group. This arrangement is sufficient to prevent percolation of bond strain in As_xSe_{1-x} alloys, and has been used to define the values of $x_c(1)$ and $r_c(1)$ at the transition from floppy to rigid. The test for this model is the determination of the value of $n_c(1)$ that corresponds to these bonding model extension for determination of $x_c(1)$ and $r_c(1)$.

A continuous random network comprised of a 2:1 mixture of As–Se–Se–As and As–Se–As bonding arrangements as in figure 2(b) has to a molecular formula representation: As_2Se_5. This gives a value of $x_c(1)$ equal to 2/7 or 0.286, and an $r_c(1) = 2.89$. These values are in excellent agreement with experiment [9]. However, based on a restricted force field of 2-body and 3-body forces, $r_c(1) = 2.29$ corresponds to a value of $n_c(1) = 2.72$, which is significantly below the threshold of 3 for a floppy to rigid transition. This is anticipated by equation (1); since $r_c(1) = 2.29$ which is less than 2.4, $n_c(1)$ must then be <3 for a valence force field comprised of 2-body bond-stretching and 3-body bond-bending valence forces [1].

The 3-fold coordination, and the non-bonding lone pairs on the As atoms, introduce additional constraining forces associated with many-body repulsive forces, e.g. as in the valence shell electron pair repulsion (VSPEPR) model for molecular structure as discussed in section 2.2 and the energy level diagrams in figures 5(a) and (b) [25, 26]. These repulsions add additional constraints, that must be included in determining the values of n_c for the onset, $n_c(1)$, as well as the value of $n_c(2)$ at the termination of the IP.

As already noted above, the value of $x_c(1) = 0.286$ corresponds to the experimentally determined onset of IP behavior at $r_c(1) = 2.29$ as determined by reversibility of heat flow, for As–Se alloys [6, 28]. The addition of one constraint/As atom to take into account lone-pair repulsions increases the number of constraints per As atom from 4.5 (1.5 stretching and 3 bending) to 5.5. This additional constraint increases $n_c(1)$ from 2.72 to 3.0 which is then consistent the onset of the first floppy to rigid transition at the beginning of IP phase at $r_c(1) = 2.29$.

The experimental value of $r_c(2)$ at the termination of the IP window 2.37; this is also below the mean-field value for IP window determined solely by 2-body stretching and 3-body bending forces, and corresponds to $x_c(2) = 0.37$. The value for $n_c(2)$ at the rigid to stressed-rigid transition that terminates the IP window has been determined by including the additional repulsive constraint for As, and is 3.3. The IP windows for As_xSe_{1-x} alloys are compared with those for $Ge_{1-x}Se_x$ alloys in figures 4(a) and (b). In the representation based on r_c scaling in 4(a), the IP window for the As_xSe_{1-x} alloys is shifted to lower values of $r_c(1)$ and $r_c(2)$ with respect to the IP window for the first IP window in the Ge_xSe_{1-x} alloys. This is consistent with adding an additional constraint to the As atoms. In contrast, the IP window for the second *proposed* Ge_xSe_{1-x} IP centered at $x \sim 0.4$ is shifted to higher values of $r_c(1)$ and $r_c(2)$ with respect to the IP window for the first IP window. This is consistent with broken bond-bending constraints on the Ge atoms within the second IP regime that includes Ge–Ge bonds in tetrahedral arrangements with reduced local site symmetry.

6. The intermediate phase in $As_xGe_xSe_{1-2x}$ alloys

The intermediate phase window, when plotted as a function r_c for $As_xGe_xSe_{1-2x}$ alloys, extends from $r_c(1) = 2.33$, and $2x_c(1) = 0.22$, to $r_c(2) = 2.45$, and $2x_c(2) = 0.30$ [6]. Since this alloy has equal Ge and As content, it is appropriate for comparisons with the Ge_xSe_{1-x} and As_xSe_{1-x} alloys to use scaling based on $2x_c(i)$, $i = 1, 2$, rather than the constituent Ge and As $x_c(i)$ values. Using the same constraint counting as for Ge, As and Se as applied respectively to Ge_xSe_{1-x} and As_xSe_{1-x} alloys, the following values are obtained for $n_c(i)$ $i = 1, 2$; $n_c(1) = 2.93$ and $n_c(2) = 3.28$. The low value for $n_c(1)$ suggests that repulsions between As and Se lone pairs in nearest-neighbor sites with Ge–Se–As sequences, cannot be neglected in these ternary alloys; these Ge–Se–As linkages are not present in either of the end-member binary alloys. Based on random alloy bonding, inclusion of the Ge–Se–As groups will increase the number of constraints per Se atom, and on average this will include at most 20% of the Se atoms. Assuming 0.5 additional constraints per Se atom, and applying this to 20% of the Se atoms increases the total number of constraints per Se atom from 2.0 to ∼2.1, yielding increases to $n_c(i)$ $i = 1, 2$: $n_c(1) = 3.00$ and $n_c(2) = 3.34$.

Figures 6(a) and (b) respectively compare the IP windows the $As_xGe_xSe_{1-2x}$ alloys with those of Ge_xSe_{1-x} and As_xSe_{1-x} alloys as functions of r_c, and n_c. With r_c as the scaling variable, the $As_xGe_xSe_{1-2x}$ alloys have an IP range that begins at a slightly higher value of $r_c(1)$ than the As_xSe_{1-x} alloys, overlaps a significant portion of the Ge_xSe_{1-x} IP window, and terminates at value of $r_c(2)$ that is smaller than the end of the r_c range for Ge_xSe_{1-x} [6]. This comparison is based on experimentally determined values of the boundaries of the $As_xGe_xSe_{1-2x}$ alloy IP window to determine the corresponding values of $x_c(1)_{Ge}$ and $x_c(1)_{As}$, and $x_c(2)_{Ge}$ and $x_c(2)_{As}$; these the same for As and Ge atoms. Similarly a value of $x_c(1)_{Ge,As} = 0.11$ for both As and Ge has been obtained from heat-flow measurements for the first transition from floppy to rigid; this corresponds to a value for $r_c(1) = 2.33$, that is intermediate between the values of 2.29 and 2.40, respectively for As_2Se_{1-x} and Ge_xSe_{1-x} alloys [29]. Similarly a value of $x_c(2)_{Ge,As} = 0.15$ for both As and Ge has been obtained from the same heat-flow measurements for the second transition from rigid to stressed rigid; this corresponds to a value for $n_c(2) = 3.34$, that is intermediate between the values of 3.30 and 3.37, respectively for As_2Se_{1-x} and Ge_xSe_{1-x} alloys. These values of $r_c(1, 2)$ and $n_c(1, 2)$ for the $As_xGe_xSe_{1-2x}$ alloys are each essentially equal to mean-field averages for the As_2Se_{1-x} and Ge_xSe_{1-x} alloys; i.e., $r_c(1)_{As-Ge-Se} = 2.33–0.5(r_c(1)_{Ge-Se} + r_c(1)_{As-Se}) = 2.34$, and $n_c(1)_{As-Ge-Se} = 3.34–0.5(n_c(1)_{Ge-Se} + n_c(1)_{As-Se}) = 3.34$.

7. The intermediate phase in $Ge_{0.25}Se_{0.75-x}I_x$ alloys

Based on heat-flow measurements, the IP window in this ternary alloy is very narrow, from approximately $x_c(1) \sim 0.165$ at the threshold from floppy to rigid, to $x_c(2) \sim 0.155$ at the second threshold from rigid to stressed rigid corresponding respectively to $r_c(1) = 2.335$ and $r_c(1) = 2.345$ [30]. Note that the Ge–Se host for the incorporation of I is $Ge_{0.25}Se_{0.75}$, or equivalently $GeSe_3$. This is the alloy composition that is very close to the end of the Ge_xSe_{1-x} alloy IP window, i.e., the transition from rigid to stressed rigid in Ge_xSe_{1-x} alloys. Including the additional bonding constraints from ES tetrahedra, as well as CS groups, at this transition, $n_c(2) \sim 3.37$.

The position of the IP window can be estimated from the Se to Ge ratios at the I concentrations that bracket this window. For the floppy to rigid regime transition, this ratio is $(0.75–0.155)/0.25 = 2.38$, corresponding to an $r_c(1) = 2.59$, and for the rigid to stress-rigid transition the Se/Ge ratio is 2.34, so that $r_c(2) = 2.60$. Each of these IP boundaries are

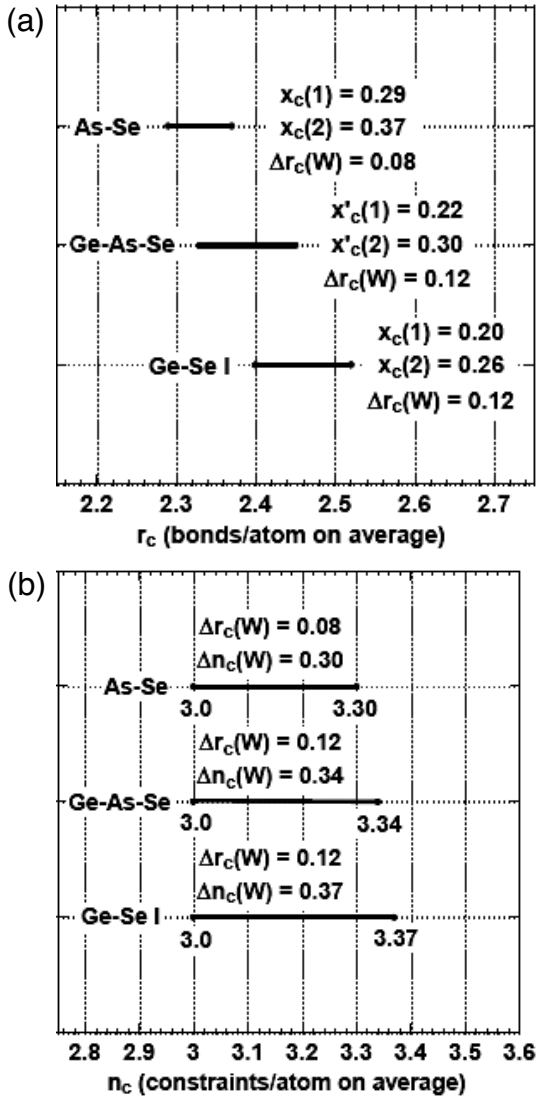

Figure 6. (a) Schematic representation of IP regimes in the Ge_xSe_{1-x}, As_xSe_{1-x} and $Ge_xAs_xSe_{1-2x}$ alloy systems (a) as function of r_c and (b) as a function of n_c.

significantly above the IP window for Ge–Se alloys, whereas the actual transition falls below the IP window for the Ge_xSe_{1-x} alloy. As expected, the r_c values are driven into the IP regime for Ge–Se alloys when the I concentration and constraints are taken into; $r_c(1)$ is reduced to 2.335, and $r_c(2)$ to 2.35, both of which fall below the first transition of the Ge–Se alloy system [6], and are close to the experimentally determined values from the reversible heat-flow measurements.

The next issue to be addressed is the following: are the I substitutions for Se at the respective concentrations of ∼0.165 at the first transition, and ∼0.155 at the second transition sufficient to define the onset and termination of an IP window with values of $n_c(1) \sim 3$ and $n_c(2) > 3$, respectively? The answer is yes, but only when the constraint counting is modified.

To perform this calculation it is necessary to take into account (i) broken constraints on the Ge atoms which are terminated with either one or two I atoms, (ii) additional constraints on Se atoms which are due to repulsions between their lone pair p-state and with the non-bonding pairs on the terminal I atoms, and finally (iii) additional constraints are added to the I atoms to taken into account repulsions involving their non-bonding pairs as well. It is important to recognize that I and other halogen terminators, F, Cl and Br are qualitatively different than H and D. For H and D, the electron density is localized in the σ-bond between these atoms and a network constituent, and equally important there are no other electrons 'belonging' to H or D atoms that are involved in repulsive interactions.

As a point of reference, based on the SEBCT theory with only bending and stretching constraints, $n_c(1) = 2.38$, and $n_c(2) = 2.40$. These values are not in accord with those required for an IP window. We assume all of the I atoms are bonded to Ge in a mono-I terminal group. This means that there are broken bond-bending constraints on 16.5% of the Ge atoms, and full bonding constraints on 8.5%. The value of n_c(Se) is increased by one to include the constraint from interactions between the Se lone pairs and the non-bonding lone pair electrons on the terminal I atoms; this is ∼1 constraint for 30% of the Se atoms, so that the average number of Se constraints is increased from 2 to 2.3. The number of constraints on the terminal I atom is comprised of 0.5 stretching constraints (for a terminal atom), and 1 additional constraint for the repulsive interactions with the Se atom non-bonding pairs and with other near-neighbor I atoms as well. Proceeding in this way the average number of constraints per atom at the floppy to rigid transition is estimated in the following calculation: $n_c(1) \sim 0.165(4.5) + 0.085(7)$ for Ge, 0.585(2.3) for Se, and 0.165(1.5) for I, so that $n_c(1) \sim 2.93$. The number of constraints/atom for the rigid to stressed-rigid transition is estimated by the same constraint counting, and $n_c(2) \sim 2.96$.

The observation that these values of n_c are less than the anticipated value of 3.00 may be related to the assumption made about the strength of the constraints added to the large I atom. The choice of 1 constraint was arbitrary and is now adjusted. The density on non-bonding electrons in lone pair orbitals is three times higher than for the lone pairs on Se or As, this should warrant an increase in the magnitude of that constraint. As an example, if the scaling were based on an increased effective constraint of 1.5, then n_c(I) would be increased to $0.5 + 1.5 \sim 2.0$, increasing $n_c(1)$ to ∼3.01 and $n_c(2)$ to ∼3.04, suggesting that this is a well-educated guess and a reasonable assumption as well.

These values are consistent with that small IP window that is present in the $r_c(1)/r_c(2)$ representation, where $\Delta r_c = 0.01$. Figures 7(a) and (b) include IP window schematic representations that compare these windows for $Ge_{0.25}Se_{0.75-x}I_x$ alloys with those for the Ge_xSe_{1-x}, As_xSe_{1-x} and $As_xGe_xSe_{1-2x}$ alloys for r_c and n_c, respectively. The relative window positions in the n_c plot in figure 7(b) suggest that the additional constraints due to the repulsive interactions on the I atoms in the Ge–Se–I alloys are more important than the broken constraints on the Ge atoms.

8. Discussion

The arguments and examples presented above for the boundaries of IP phases in Se-based binary and ternary alloys are based on the introduction of an expanded force field for constraints that includes longer range repulsive interactions in the spirit of the VSEPR model [14], as well as broken bending constraints as originally discussed in [10]. In addition, the IP widows between the transitions between floppy and rigid, and rigid and stressed rigid have also been displayed using n_c as scaling comparison parameter in addition to the traditional approach of Boolchand which relied primarily on r_c [6]. Comparisons between the r_c and n_c plots

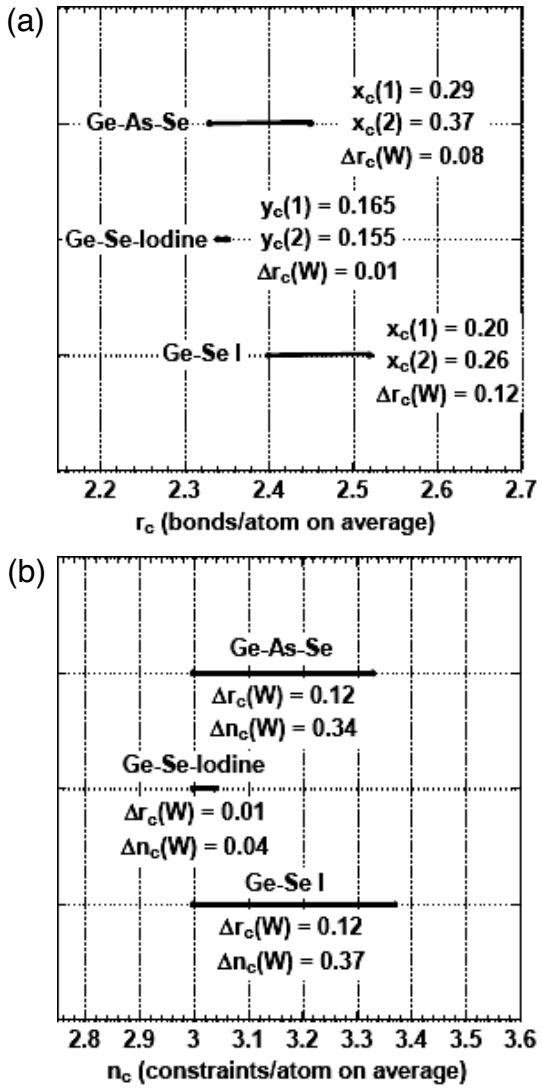

Figure 7. (a) Schematic representation of IP regimes in the Ge_xSe_{1-x}, As_xSe_{1-x} and $Ge_{0.25}Se_{0.75-x}I_x$ alloy systems as functions of (a) r_c and (b) n_c.

provide important insights in the importance of broken bond-bend constraints, and additional constraints due to many-body repulsive effects associated with non-bonding lone-pair electrons of the As, Se and halogen I alloy atoms as well.

Other alloy systems have also been studied by Boolchand and co-workers; e.g. the IP windows are different for S containing alloys As_xS_{1-x} and $Ge_xAs_xS_{1-2x}$, as compared respectively to As_xSe_{1-x} and $Ge_xAs_xSe_{1-2x}$. The position of the first transition for these alloys is shifted to lower values of $x_c(1)$, or equivalently to smaller values of $r_c(1)$. This has been attributed by the Boolchand group to the diphasic character of low As, or Ge + As content in the As_xS_{1-x} and $Ge_xAs_xS_{1-2x}$ alloys respectively. These alloys contain S_8 molecules that have been detected in Raman spectroscopy, and are not included in the network phase. As such the

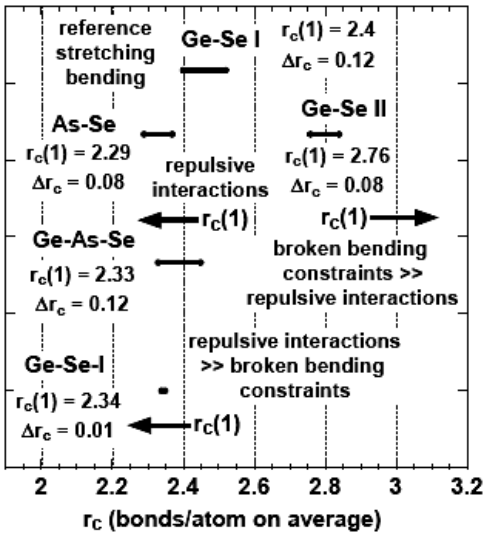

Figure 8. Schematic representation of IP regimes in the Ge_xSe_{1-x}, As_xSe_{1-x}, $Ge_xAs_xSe_{1-2x}$ and $Ge_{0.25}Se_{0.75-x}I_x$ alloy systems as function of r_c. Marked arrows and text indicate the different shifts in r_c (1) associated with broken bonding–bending constraints, and repulsive interactions.

first floppy to rigid transition is shifted to lower energy. This also has consequences for the CBSOs, and the values of $r_c(2)$ and $n_c(2)$ that mark the second transition. One exception to this is the ternary alloy system $Ge_{0.25}S_{0.75-x}I_x$, in which the floppy to rigid, and rigid to stressed rigid transitions occur at the same values of x_c, r_c and n_c as for the $Ge_{0.25}S_{0.75-x}I_x$ alloys. This is a manifestation of the Ge concentration of 25%, which combined with the I concentrations moves thus alloy out of a regime where S_8 molecules are a second phase.

Figure 8 summaries the effects of additional bonding constraints due to either (i) repulsive interactions between lone-pair orbitals on 2-fold and 3-fold coordinated atoms such as S and Se, and As and P, respectively, and/or halogen atom bond terminators such as F, Cl, Br and I, and (ii) broken bond-bending constraints on 4-fold coordinated atoms such as Si and Ge. The original formulation of SEBCT was based on an assumption that 2-body and 3-body, bond-stretching and bond-bending forces, respectively contributed to local bond strain [1, 2]. This approximation applies to the first IP in the Ge_xSe_{1-x} alloy, where the constraints that determine the number of bonds/atom on average, $r_c(1)$, and bonding constraints/atom on average, $n_c(1)$ are 2.4 and 3, respectively, in accord with the SEBCT model. The plot in figure 8 uses the Ge–Se alloy, designated as Ge–Se, as reference system for understanding the effects of the additional bonding constraints noted above on the $r_c(1)$ value for the first transition between a floppy and rigid, but not stressed IP regime. As shown in the figure, the incorporation of broken bond-bending constraints for the second possible Ge_xSe_{1-x} IP window, designated as Ge–Se II, and centered at a value of $x_c \sim 0.4$ shifts the IP regime to higher value of r_c. The $r_c(1)$ value is increased from 2.4 for 2- and 3-body bond-stretching and bond-bending constraints >2.75, when broken constraints on the Ge atoms are taken into account due to the inclusion of Ge–Ge bonds in addition to Ge–Se bonds.

An important aspect of figure 3(a) is the effect of forces other than 2- and 3-body valence forces on the $r_c(1)$ values that mark the onset of the IP regime. The first example, Ge–Se II, has demonstrated that when bond-bending constraints dominate, they shift the first transition for the beginning of IP window to higher values of $r_c(1)$ greater than 2.4. The effects of repulsive interactions have the opposite effect, shifting $r_c(1)$ to values less than 2.4. This is illustrated

Table 1. Application of mean-field bonding in the stressed-rigid alloy regimes to identify the double percolation pathways in the respective IP regimes.

Alloy	Compliant bonding group	Stressed-rigid bonding group	Calculated stressed-rigid concentration, $x_c(2)_{cal}$	Experimental stressed-rigid concentration, $x_c(2)_{exp}$
Ge–Se I	$GeSe_4$	$GeSe_2$	$x_c(2)_{cal} = 2/8$	
	Ge–Se–Se–Ge	Ge–Se–Se	$x_c(2)_{cal} = 0.25$	$x_c(2)_{exp} = 0.26$
Ge–Se II	Ge_2Se_3	GeSe	$x_c(2)_{cal} = 3/7$	
	$_3$Se–Ge–Ge–Se_3	Ge–Se	$x_c(2)_{cal} = 0.43$	$x_c(2)_{exp} = 0.43$
As–Se	As_2Se_5	As_2Se_3	$x_c(2)_{cal} = 4/12$	
	$_2$As–Se–Se–As_2	As–Se–As	$x_c(2)_{cal} = 0.33$	$x_c(2)_{exp} = 0.33$
Ge–As–Se[a]	$2As_2Se_5$	$2As_2Se_3$	[b] $x'_c(2)_{cal} = (0.667 + 25)/3$	
	$1GeSe_4$	$1GeSe_2$	$x'_c(2)_{cal} = 0.31$	$x_c(2)_{exp} = 0.30$

[a] Assumes a compliant pathway with As and/or Ge connected through Se–Se dimer groups of two atoms, and a stressed-rigid-stressed pathway with As and/or Ge connected through a single monomer Se atom.
[b] $x'_c(2) = (2x_c(2)\text{As–Se} + x_c(2)\text{Ge–Se})/3$.

by the values of $r_c(1)$ for the floppy to rigid transitions in the alloys systems designated as As–Se and Ge–As–Se where there are no broken bond-bending constraints. In the Ge–Se–I system there are both broken bond-bending constraints, and repulsive effects as well; however, the repulsive effects dominate, and the shift in $r_c(1)$ is to values of $r_c(1)$ smaller than 2.4.

Moving on, it is important to note that electronic structure calculations have demonstrated that total energy is essentially independent of the dihedral angle that defines for orientation of the σ-bonds on the pairs of 4-fold coordinated Ge or Si that bridge O or S atoms in 4–2 alloys such as GeO_2SiO_2 and GeS_2 [25, 26]. In contrast, for the 3–2 alloys such as As_2O_3 and As_2S_3, repulsive forces, and bond strain derived from repulsions involving lone-pair electrons on each of constituent atoms favors a staggered orientation of non-bonding pairs on the As atoms rather than eclipsed orientations [25, 26]. This result has been found in *ab initio* calculations of optimized bond angles and IR effective charges determined from configuration interaction (CI) methods for ground state configurations, as well structural relaxation after optical excitations that gives rise to photo-darkening and photo-structural changes in As_2S_3 and GeS_2 [31, 32]. Representative results from these electronic structure calculations have been displayed in figures 5(a) and (b) for ground state effects.

The extension of SEBCT to include broken constraints also explains why intermediate phases are important in other thin film materials for device applications. These include (i) a-Si(H) in solar cells and thin film transistors, (ii) the SiO interfacial transition region between crystalline Si and a-SiO_2 in field effect transistors, (iii) a-Si,N,H alloys in thin film transistor gate dielectrics, and finally, (iv) a newly discovered medium-k gate dielectric that is allowing the continuance of Moore's law scaling for at least 2 more generations of complementary metal oxide semiconductor CMOS, circuits and systems [6, 10]. Finally, the observation noted above that ternary alloy metrics for average number of bonds/atom at the two transitions that mark the beginning and end of the IP in the As–Ge–Se system are mean-field averages of the same mean-field properties of the relevant binary alloys systems, As–Se and Ge–Se. This suggests that CBSOs take place *in parallel* and that *double percolation* effects may indeed contribute [33]. Double percolation, a well-established phenomenon in polymer blend–carbon black composites [34, 35], then has the potential to provide another more general framework to cast the results of the chemical bonding oriented approach of this paper.

The validity of the double percolation approach is illustrated in table 1, where we have extended the discussion of the percolation model of bonding in the first IP regime of Ge–Se I

(the first IP window in the Ge_xSe_{1-x} alloy system) to the Ge–Se II, As–Se and Ge–As–Se alloy IP windows to estimate the value of x_c (2) at the end of these respective IP windows. In each of these alloy systems we identify the compliant bonding arrangement that is associated with the floppy regime, e.g. Ge–Se–Se–Ge groups for Ge–Se I, and the stressed rigid group that has completely percolated in the stressed-rigid regime, in this example Ge–Se–Ge. Proceeding in this way the values of the second threshold concentration, $x_c(2)_{cal}$, in the table estimated from the threshold of percolation stressed rigid behavior in a cluster Bethe Lattice approximation, 50% of bonding groups, above the second IP window gives values of $x_c(2)_{cal}$ very close the experimentally determined window limit, $x_c(2)_{exp}$. For the two primary IPs (Ge–Se I and As–Se) in the binary systems, this value of $x_c(2)_{exp}$ is half-way between the experimentally determined threshold for the beginning of the IP phase, $x_c(1)_{exp}$, and the first stoichiometric composition within the stressed rigid regime. For the second IP in the alloy system (Ge–Se II) it is between the $x_c(1)_{exp}$ and the stoichiometric compound GeSe. For the Ge–As–Se alloy system, which has a weighting factor of 1:2 for the ratio of the Ge–Se component to the As–Se component, the same relationship applies, but with appropriately weighted end-member pseudo-compound ($GeSe–As_2Se_3$).

Acknowledgments

This work has been supported by the Office of Naval Research, the Semiconductor Research Corporation, and Air Force Office of Scientific Research. It has also benefited significantly from discussions with Professor M F Thorpe at Arizona State University, Professor Punit Boolchand at the University of Cincinnati.

References

[1] Phillips J C 1979 *J. Non-Cryst. Solids* **34** 153
[2] Kerner R and Phillips J C 2001 *Solid State Commun.* **17** 47
[3] Lucovsky G and Phillips J C 2000 *J. Non-Cryst. Solids* **266** 1335
[4] Lucovsky G and Phillips J C 2004 *J. Vac. Sci. Technol.* B **22** 2089
[5] Lucovsky G, Baker D A, Paesler M A and Phillips J C 2007 *J. Non-Cryst. Solids* **353** 722
[6] Maxwell J C 1864 *Phil. Mag.* **27** 294
[7] Jacobs D J and Thorpe M F 1995 *Phys. Rev. Lett.* **75** 22
[8] Wang F, Mamedov S, Boolchand P, Goodman B and Chandrasekhar M 2005 *Phys. Rev.* B **71** 174201
[9] Wang F and Boolchand P 2004 *Non-Crystalline Materials for Optoelectronics* ed G Lucovsky and M Popescu (Romania: INOE) chapter 2, p 15
[10] Lucovsky G and Phillips J C 2004 *Appl. Phys.* A **78** 453
[11] Lucovsky G, Nemanich R J and Galeener F L 1977 *Proc. 7th Int. Conf. on Amorph. Liquid Semconduct. (University of Edinburgh, Edinburgh)* p S. 130
[12] Baker D A, Paesler M A, Lucovsky G and Taylor P C 2006 *J. Non-Cryst. Solids* **352** 1621
[13] Nakamoto K 1997 *Infrared and Raman Spectra of Inorganic and Coordination Compounds, Part A* (New York: Wiley Interscience) section 2
[14] Cotton F A and Wilikinson G 1972 *Advanced Inorganic Chemistry* 3rd edn (New York: Interscience) chapter 3
[15] Shriver D and Atkins P 1999 *Inorganic Chemistry* 3rd edn (New York: Freeman) chapter 3
[16] Lucovsky G and Wong C K 1985 *J. Non-Cryst. Solids* **75** 51
[17] Boolchand P, Feng X and Bresser W J 2001 *J. Non-Cryst. Solids* **293** 348
[18] Feng X, Bresser W J and Boolchand P 1997 *Phys. Rev. Lett.* 442
[19] Nemanich R J, Solin S A and Lucovsky G 1977 *Solid State Commun.* **21** 273
[20] Wong C K, Lucovsky G and Bernholc J 1987 *J. Non-Cryst. Solids* **97/98** 1171
[21] Boolchand P, Lucovsky G, Phillips J C and Thorpe M F 2005 *Phil. Mag.* **85** 3823
[22] Sartbaeva A, Wells S A, Huerta A and Thorpe M F 2007 *Phys. Rev.* B **75** 224204
[23] Lucovsky G, Galeener F L, Keezer R C, Geils R H and Six H A 1974 *Phys. Rev.* B **10** 5134
[24] Zallen R 1983 *The Physics of Amorphous Solids* (New York: Wiley Interscience) chapter 7

[25] Whitten J L, Zhang Y, Menon M and Lucovsky G 2002 *J. Vac. Sci. Technol.* B **20** 1710
[26] Lucovsky G, Mowrer T, Sremaniak L S and Whitten J L 2004 *J. Non-Cryst. Solids* **338–340** 155
[27] Papatheodorou G N and Solin S A 1976 *Phys. Rev.* B **13** 1741
[28] Georgiev D G, Boolchand P and Micoulaut M 2000 *Phys. Rev.* B **62** R9228
[29] Wang Y, Boolchand P and Micoulaut M 2000 *Europhys. Lett.* **52** 663
[30] Boolchand P, Georgiev D G and Goodman B 2001 *J. Optoelectron. Adv. Mater.* **3** 703
[31] Mowrer T, Lucovsky G, Sremaniak L S and Whitten J L 2004 *J. Non-Cryst. Solids* **338–340** 543
[32] Lucovsky G and Paesler M A 2004 *Non-Crystalline Materials for Optoelectronics* ed G Lucovsky and M Popescu (Romania: INOE) chapter 7, p 325
[33] Lucovsky G and Phillips J C 2007 *J. Phys.: Condens. Matter* **19** 455219
[34] Levon K, Margolina A and Patashinsky A Z 1993 *Macromol.* **26** 4061–3
Gubbels F, Blacher S, Vanlathem E, Jerome R, Deltour R, Brouers F and Teyssie P 1995 *Macromol.* **28** 1559–66
[35] Moraal H 1995 *J. Phys. A: Math. Gen.* **28** 2745–58